Complex antipolar $\sqrt{2} \times 4 \times 2\sqrt{2}$ structure with *Pnma* symmetry in $BiFeO_3$ and $BiFe_{1/2}Sc_{1/2}O_3$: First-principles calculations

Sergey A. Prosandeev,[1,2] Dmitry D. Khalyavin,[3,*] Igor P. Raevski,[2] Andrei N. Salak,[4] Nikolai M. Olekhnovich,[5] Anatoly V. Pushkarev,[5] and Yury V. Radyush[5]

[1]*Physics Department, University of Arkansas, Fayetteville, Arkansas 72701, USA*

[2]*Faculty of Physics and Research Institute of Physics, Southern Federal University, 344090 Rostov-on-Don, Russia*

[3]*ISIS facility, STFC, Rutherford Appleton Laboratory, Chilton, Didcot, Oxfordshire OX11-0QX, United Kingdom*

[4]*Department of Materials and Ceramic Engineering/CICECO, University of Aveiro, 3810-193 Aveiro, Portugal*

[5]*Scientific-Practical Materials Research Centre of NAS of Belarus, Minsk 220072, Belarus*

(Received 23 April 2014; revised manuscript received 24 July 2014; published 18 August 2014)

First principles calculations are done for a $\sqrt{2} \times 4 \times 2\sqrt{2}$ *Pnma* structure, which has been recently discussed in several attempts to describe experiments in complex magnetoelectric perovskites and which experimentally was shown to compete with several ferroelectric phases. This makes these materials extremely attracting as switchers, starters, field-stimulated capacitors, high-voltage converters, transmitters, etc. The relative energies of the $\sqrt{2} \times 4 \times 2\sqrt{2}$ *Pnma* structure have been calculated from first principles and analyzed as a function of pressure in $BiFeO_3$. The stability of two polymorphs of the $\sqrt{2} \times 4 \times 2\sqrt{2}$ *Pnma* structure has been studied for solid solution $BiFe_{1/2}Sc_{1/2}O_3$. The main distortions and relative energies of these two polymorphs in $BiFe_{1/2}Sc_{1/2}O_3$, in terms of $Pm\bar{3}m$ parent symmetry, have been calculated from first principles as well.

DOI: 10.1103/PhysRevB.90.054110 PACS number(s): 75.25.−j

A few publications recently reported the emergence in several magnetoelectrics such as (Bi,La)FeO_3 [1], $BiFe_{0.75}Mn_{0.25}O_3$ [2], $BiFe_{1/2}Sc_{1/2}O_3$ [3], and (Bi,Nd)FeO_3 [4,5] of a $\sqrt{2} \times 4 \times 2\sqrt{2}$ antipolar structure with *Pnma* symmetry (the superstructure is specified in terms of the pseudocubic perovskite cell) competing with ferroelectric structures of *R*3*c* and other symmetries. This antipolar structure has a rather interesting rotational octahedra (tilting) pattern of "$++--$" type, where "+" stays for the clockwise and "−" for counterclockwise rotation of the oxygen octahedra, about the $[010]_p$ axis. A similar rotational pattern was observed in $BiScO_3$ thin films on $SrTiO_3$ [6], in (CaSr)TiO_3 [7], and in $AgNbO_3$ [8].

In contrast to these references, a similar "$++--$" pattern was found to be polar [8]. A polar rotational structure of the "$++--$" type was studied in first-principles calculations of $BiFeO_3$ (BFO) [9] under pressure. Polar and nonpolar structures with symmetry different from *Pnma* were discovered in first-principles calculations of $EuTiO_3$ [10]. The latter two calculations were done for $\sqrt{2} \times \sqrt{2} \times 4$ and even longer supercells, along axis *c*, for example $\sqrt{2} \times \sqrt{2} \times 6$, which are consistent with recently found long rotational patterns in $NaNbO_3$ [11]. A complex twin structure is expected at morphotrophic phase boundaries of some solid solutions [12,13]. It has been realized recently that the common mechanism for the formation of such a complex twinned structure can be explained by flexoelectric interactions [14,15].

To the best of our knowledge, first-principles calculations of the $\sqrt{2} \times 4 \times 2\sqrt{2}$ antipolar structure of *Pnma* symmetry have not yet been performed. The natural goal of the present study is to perform such calculations and to analyze the result from the symmetry and enthalpy (energy) points of view.

We will consider two examples. One is the recently intensively studied magnetoelectric BFO under hydrostatic pressure [9,16–18]. Specifically, we will investigate the change of the stability of this complex $\sqrt{2} \times 4 \times 2\sqrt{2}$ antipolar *Pnma* structure versus pressure, with respect to other polar and nonpolar structures. The importance of this study is confirmed by the fact that BFO at low pressure and low temperature shows a polar *R*3*c* symmetry, while under high pressure it converts into an orthorhombic antipolar $\sqrt{2} \times 2 \times \sqrt{2}$ structure with *Pnma* symmetry [16]. Between these two phases, experiment found a more complex pattern, which has not been identified so far, although first-principles calculation of the volume of the polar $\sqrt{2} \times 4 \times \sqrt{2}$ "$++--$" twin fitted experimental results well [9].

At the same time, several experimental investigations are known for (*R*Bi)FeO_3, where *R* stands for rare-earth elements. For example, solid solutions of BFO with $SmFeO_3$ [19] showed transformation of the polar *R*3*c* structure of BFO into the orthorhombic $\sqrt{2} \times 2 \times \sqrt{2}$ *Pnma* structure inherent to $SmFeO_3$. Between these two phases, experiment [19] revealed the existence of a more complex structure, which was probably close to the *Pbam* structure of $PbZrO_3$. Later, a similar structure in the solid solution of BFO and $NdFeO_3$ was identified as a $\sqrt{2} \times 4 \times 2\sqrt{2}$ structure with *Pnma* symmetry [5]. Very probably, one may expect the same result for the intermediate phase in pure BFO under pressure, because such hydrostatic pressure is akin to the chemical pressure in (*R*Bi)FeO_3 solid solutions. We are not aware about any first-principles calculations of this pattern.

The other target for our analysis is the solid solution $BiFe_{1/2}Sc_{1/2}O_3$ (BFS), where presence of the antipolar $\sqrt{2} \times 4 \times 2\sqrt{2}$ *Pnma* pattern was also evidenced from x-ray and neutron diffraction experiments [3]. It was shown in this study that there exist two possible polymorphs of the *Pnma* symmetry differing by the origin of the modes, in terms of the $Pm\bar{3}m$ cubic symmetry.

*dmitry.khalyavin@stfc.ac.uk

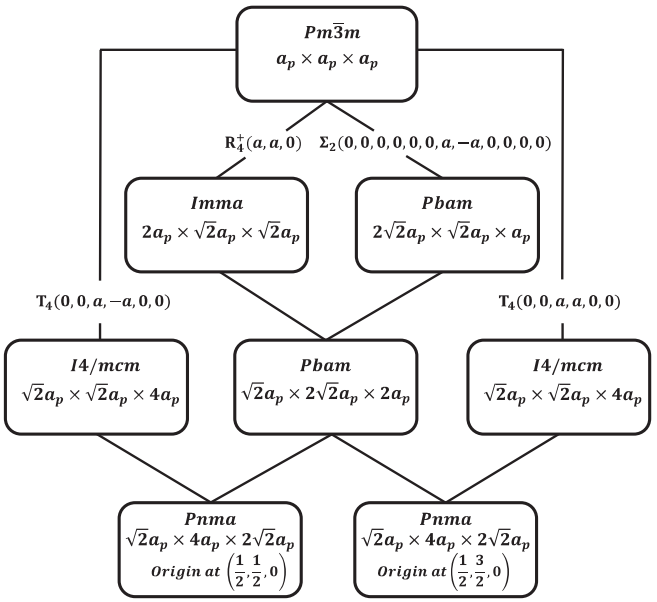

FIG. 1. A scheme of the formation of the $\sqrt{2} \times 4 \times 2\sqrt{2}$ *Pnma* phase as a distortion of the $Pm\bar{3}m$ cubic structure (all axis lengths are given in terms of the cubic cell).

Figure 1 shows the scheme of the formation of the two different polymorphs of the $\sqrt{2} \times 4 \times 2\sqrt{2}$ *Pnma* supercell as a result of the distortion of the $Pm\bar{3}m$ cubic structure. The R_4^+, Σ_2, and T_4 order parameters represent anti-phase octahedral tilting about the $[101]_p$ axis, antiferroelectric displacements along the $[101]_p$ axis, and "$++--$" or "$+--+$" octahedral tilting about the $[010]_p$ axis, respectively [20,21]. The "$++--$" and "$+--+$" tilting patterns imply different origin choice and correspond to the (0,0,a, $-a$,0,0) and (0,0,a,a,0,0) directions in the T_4 representation space. Combination of the distortions of the R_4^+ oxygen octahedra tilting and Σ_2 antiferroelectric Bi displacements creates the $\sqrt{2} \times 2\sqrt{2} \times 2$ *Pbam* structure specific to $PbZrO_3$ [22]. Further mixture of the *Pbam* distortion with the T_4 oxygen octahedra tilting results in the two polymorphs of the $\sqrt{2} \times 4 \times 2\sqrt{2}$ *Pnma* structure, depending on the two possible origins for the T_4 mode. It was not possible to deduce from the experiment which of these two modifications was stable and which was metastable in the BFS solid solution. We will answer this question on the basis of our first-principles calculations, and we will investigate the difference between these two *Pnma* structures at the microscopic level. We will also investigate the dependence of the energy of this structure on the exchange-correlation (XC) functional employed and on the chemical configuration of the Fe and Sc ions.

We performed first-principles calculations of BFO in the framework of density functional theory (DFT) [23] within the local density approximation (LDA) + U method [24] by using the Vienna *ab initio* simulation package (VASP) [25]. We employed the Hubbard parameter $U = 3.8$ eV, as calculated for Fe ions in BFO in Ref. [26]. In the present study, we utilized the projected augmented wave (PAW-PBE) method [27] as implemented in VASP [25] and which has been used already in calculations of complex twins in BFO [9]. An 80-ion

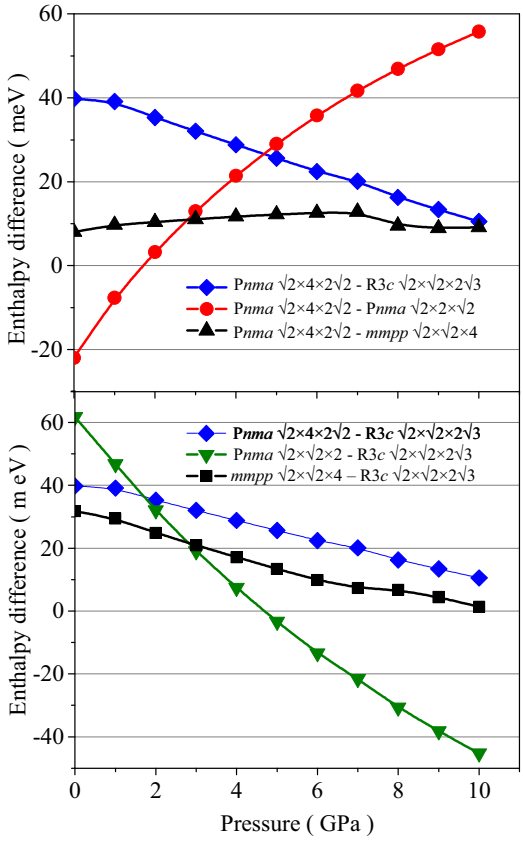

FIG. 2. (Color online) (a) Enthalpy difference of the $\sqrt{2} \times 4 \times 2\sqrt{2}$ *Pnma* phase in BFO relative to the polar $\sqrt{2} \times \sqrt{2} \times 2\sqrt{3}$ *R*3*c*, antipolar $\sqrt{2} \times \sqrt{2} \times 2$ *Pnma* and "mmpp" (Ref. [9]) phases, as a function of hydrostatic pressure. (b) Enthalpy difference of the $\sqrt{2} \times 4 \times 2\sqrt{2}$ *Pnma*, $\sqrt{2} \times \sqrt{2} \times 2$ *Pnma*, and "mmpp" (Ref. [9]) phases in BFO relative to the *R*3*c* phase, as a function of hydrostatic pressure.

$\sqrt{2} \times 4 \times 2\sqrt{2}$ *Pnma* supercell was considered. We used the energy cutoff at 500 eV. We found the ground state crystal structure by means of energy minimization, until a precision of 10^{-5} eV was achieved. The ground state magnetic state proves to be antiferromagnetic, of G type. The calculations at finite pressure were done by employing the PSTRESS flag as implemented in VASP [25], which allows one to perform self-consistent minimization of enthalpy $H = E + PV$.

As the starting coordinates in the structural relaxation of two polymorphs [with the origin choice at (1/2,1/2,0) and (1/2,3/2,0)] of the $\sqrt{2} \times 4 \times 2\sqrt{2}$ *Pnma* phase of BFO, we employed experimental data obtained for BFS [3] (see Tables 1s and 3s of the supplemental material of Ref. [3]). The latter modification [with the origin at (1/2,3/2,0)] was found to have a lower enthalpy than the first one, in the whole studied interval of pressure between 0 and 10 GPa (we will discuss these two polymorphs below in detail for BFS, where experimental data are available for comparison). Referring further to the $\sqrt{2} \times 4 \times 2\sqrt{2}$ *Pmna* phase of BFO, we will always assume the ground state modification, with the origin at (1/2,3/2,0).

Figure 2(a) presents the enthalpy of BFO, obtained for the $\sqrt{2} \times 4 \times 2\sqrt{2}$ *Pnma* phase relative to three phases. One

phase is polar, and this is the ground state of BFO at low pressure and low temperature. The symmetry of this phase is $R3c$. The second phase is antipolar, and this phase describes the symmetry of BFO at high pressure, 10 GPa, and low temperature. The symmetry of this phase is $\sqrt{2} \times \sqrt{2} \times 2$ $Pnma$. The third and last phase is a polar twin structure with a $\sqrt{2} \times \sqrt{2} \times 4$ "mmpp" tilting pattern along the $[001]_p$ axis of the $Pm\bar{3}m$ phase (we use this abbreviation, "mmpp," as it was introduced in Ref. [9], from where we took the values of enthalpy of this phase; this abbreviation means the same as "$--++$," which we are using in the present paper). One can see that, at zero pressure, the polar $R3c$ phase is indeed the ground state, in line with experiment, and the $\sqrt{2} \times 4 \times 2\sqrt{2}$ $Pnma$ phase enthalpy decreases with respect to the enthalpy of this polar phase, as pressure increases. On the other hand, the $\sqrt{2} \times \sqrt{2} \times 2$ $Pnma$ phase is the ground state at high pressure of 10 GPa. Relative to this phase, the enthalpy of the $\sqrt{2} \times 4 \times 2\sqrt{2}$ $Pnma$ phase increases with pressure increase. It follows from Fig. 2(a) that the $\sqrt{2} \times 4 \times 2\sqrt{2}$ $Pnma$ phase has minimal energy difference with respect to these two phases, $R3c$ and $\sqrt{2} \times \sqrt{2} \times 2$ $Pnma$, at about 5 GPa, where experiment [16] shows the presence of the intermediate phase. However, our calculation does not confirm that this complex phase is ever the ground state. Moreover, the comparison of our result with that obtained in Ref. [9] is in favor of the "mmpp" phase, which has enthalpy lower than the enthalpy of the $\sqrt{2} \times 4 \times 2\sqrt{2}$ $Pnma$ phase, in the whole pressure interval studied. At the same time, both the "mmpp" and $\sqrt{2} \times 4 \times 2\sqrt{2}$ $Pnma$ phases have extremely low relative enthalpy, as follows from Fig. 2(b), where we show the enthalpy of the $\sqrt{2} \times \sqrt{2} \times 2$ $Pnma$, $\sqrt{2} \times 4 \times 2\sqrt{2}$ $Pnma$, and $\sqrt{2} \times \sqrt{2} \times 4$ "mmpp" phases (the latter values are taken from Ref. [9]) with respect to the enthalpy of the $R3c$ phase. One can see that the $\sqrt{2} \times \sqrt{2} \times 2$ $Pnma$ phase becomes the ground state above 5 GPa, while both the $\sqrt{2} \times 4 \times 2\sqrt{2}$ $Pnma$ and $\sqrt{2} \times \sqrt{2} \times 4$ "mmpp" phases are never the ground states.

Besides pure BFO, we have analyzed the structure of the solid solution BFS. When calculating this composition, we have employed four different XC functionals: PAW-GGA, PAW-LDA, PAW-PBE, and PAW-PBEsol [25], in order to investigate the stability of the result obtained. Other details are the same as in the calculation of BFO, but in this case we should distribute somehow Fe and Sc over the same perovskite positions. Since we cannot mix the different functionals for the magnetic and nonmagnetic ions, we selected two different important configurations. One of them is such that the global $Pnma$ symmetry of the crystal is saved. This possibility can be implemented because the $\sqrt{2} \times 4 \times 2\sqrt{2}$ $Pnma$ symmetry allows two different Wyckoff positions for the Fe and Sc ions and one can distribute these atoms over those different positions. The Fe ions organize in this case some compact bars possessing antiferromagnetic structures. Similar compact structures of Fe ions were recently shown to organize the ground state in $PbFe_{1/2}Nb_{1/2}O_3$ [28]. The other chemical configuration which we employed, is the rocksalt configuration of Sc and Fe. However, in the latter case, the orthorhombic $Pnma$ symmetry is not saved and is lowered to monoclinic $P2_1/c$ symmetry (even if this structure is not relaxed). This fact is interesting, and can be used to check the distribution of the Fe and Sc ions by looking at the monoclinic distortion of the lattice. If such distortion is absent, one can expect the former chemical configuration.

TABLE I. Energy (in eV) of two polymorphs of BFS with $\sqrt{2} \times 4 \times 2\sqrt{2}$ $Pnma$ symmetry and calculated from first principles with the use of different DFT functionals: GGA, LDA, PBE, and PBEsol [25,27]. "frozen" means the frozen shape of the crystal taken from experiment [3]. "rel" means the fully relaxed structure with no restrictions. "BFS1" and "BFS2" denote two different polymorphs of BFS (see below). $P2_1/c$ denotes the structure of BFS with rocksalt distribution of Fe and Sc. The difference of energy with respect to the $\sqrt{2} \times 4 \times 2\sqrt{2}$ $Pnma$ phase of the BFS2 ground state is given for the fully relaxed structures.

	GGA	LDA	PBE	PBEsol
BFS1-frozen	−546.929	−605.470	−545.785	−539.058
BFS2-frozen	−547.653	−606.385	−546.458	−539.906
delta-frozen	−0.725	−0.915	−0.674	−0.848
BFS1-rel	−547.138	−606.487	−546.165	−539.247
BFS2-rel	−547.862	−607.198	−546.862	−540.000
delta-rel	−0.724	−0.711	−0.698	−0.753
$P2_1/c$-frozen	−546.533	−605.081	−545.280	−538.568
$P2_1/c$-rel	−546.648	−605.970	−545.550	−538.671
$P2_1/c$-$Pnma$-rel	1.214	1.228	1.312	1.329

We follow the finding [3] that $\sqrt{2} \times 4 \times 2\sqrt{2}$ $Pnma$ structure has, in reality, two different realizations differing by the origin of the modes, in terms of $Pm\bar{3}m$ symmetry. We have calculated the enthalpy of both structures, which we denote as "BFS1" and "BFS2." They correspond to the experimentally found coordinates [3] of BFS with the origin choice at (1/2,1/2,0) and (1/2,3/2,0), respectively. The difference between these two structures will be discussed below. We have calculated these two structures under the condition of the frozen, experimentally found geometry of the crystal [3], and we denoted these results as "BFS-frozen." Table I shows the difference between these two energies as "delta-frozen." We calculated this difference for four different LDA+U functionals, as described above. One can see that this difference favors "BFS2" as the ground state, independently of the DFT functional.

Then, similarly, we calculated the result under the condition of the full relaxation of the lattice with no restriction imposed on the shape of the unit cell, but with the global $Pnma$ space symmetry. We denoted these energies as "BFS1-rel" and "BFS2-rel." The difference of these energies is given as "delta-rel." One can see that this difference is, again, in favor of "BFS2" as the ground state. Thus, on the basis of our first-principles calculations, we conclude that, among two BFS structures considered, the "BFS2" polymorph is the ground state, while the energy difference between them is small. Below, we will discuss the difference between these polymorphs, at the microscopic level.

In order to give a good start to experimentalists and theoreticians treating the $\sqrt{2} \times 4 \times 2\sqrt{2}$ $Pnma$ structure, we list in Tables 1S and 2S of the Supplemenatal Material [29] the "frozen" (frozen shape) and "rel" (fully relaxed) coordinates

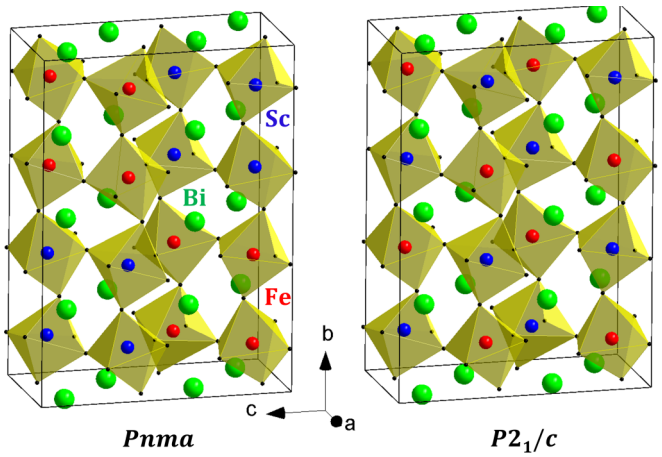

FIG. 3. (Color online) Two types of Fe and Sc cation arrangements considered in the present DFT calculation, in the $\sqrt{2} \times 4 \times 2\sqrt{2}$ *Pnma* supercell of BFS tested. One of them preserves *Pnma* symmetry (left), the other (NaCl-type) reduces the symmetry down to monoclinic $P2_1/c$ (right).

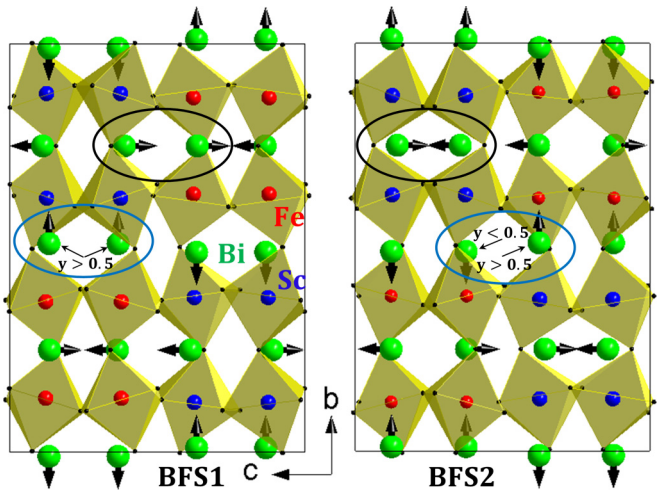

FIG. 4. (Color online) Bi-displacive modes (shown by arrows on Bi ions) doubling the *c* axis of the *Pbam* space group, incorporated into the tilted $PbZrO_3$ perovskite structure in two nonequivalent ways. One of them results in the "BFS1" structure (left panel) and the other in "BFS2" structure (right panel), both with the *Pnma* symmetry. The difference becomes clear if one compares the Bi displacements in the regions, marked with ellipses, where octahedra are tilted in a similar way.

in the "BFS2" polymorph, obtained with the help of the generalized gradient approximation (GGA) XC functional (this functional gives results a little bit closer to experiment than the others, as we will show below).

Note, that, in the calculations presented in Table I, we employed two different chemical configurations. The calculations denoted as "BFS1" and "BFS2" have a chemical configuration that saves the overall *Pnma* symmetry: we simply populated two crystallographically nonequivalent B-site positions with Fe and Sc, as shown in Fig. 3 (left). Different B sites are indicated by different colors.

The other chemical configuration we considered is akin to NaCl structure, which lowers the *Pnma* symmetry down to the monoclinic $P2_1/c$ symmetry. In Table I, the notation "$P2_1/c$-frozen" shows the result at frozen experimental geometry, and "$P2_1/c$-rel" presents the totally structurally relaxed result, with the chemical configuration of rocksalt type. One can see that the difference in energy of the "$P2_1/c$-rel" structure relative to the "BFS2-rel" structure is positive, which means that the rocksalt chemical configuration is not that preferable; rather, the $\sqrt{2} \times 4 \times 2\sqrt{2}$ *Pnma* configuration showing *G*-type magnetic coupling of the Fe ions and the origin at (1/2,3/2,0) is most stable (recall that this configuration has rather inhomogeneous distribution of the Fe and Sc ions).

The existence of the two nonequivalent structures with the $\sqrt{2} \times 4 \times 2\sqrt{2}$ supercell and *Pnma* symmetry can be clearly demonstrated using the close relation between these polymorphs and the antipolar $PbZrO_3$ structure. The latter adopts *Pbam* space group with the $\sqrt{2} \times 2\sqrt{2} \times 2$ supercell and combines both antiferroelectric displacements of Pb and octahedral tilting about the $[101]_p$ pseudocubic direction (Fig. 1). Distortions which double the *c* axis of the $PbZrO_3$ structure (pseudocubic $[010]_p$ direction) are classified by the irreducible representations associated with the *Z* ($k = 0,0,1/2$) point of the *Pbam* Brillouin zone. Two isotropy subgroups conjugated with the Z_4^+ and Z_3^- one-dimensional representations share identical *Pnma* space groups and the basis vectors (1,0,0)(0,0,2)(0, − 1,0) [20,21]. The difference applies to the origin choice, namely (0,0,0) and (0,0,1/2) for the Z_4^+ and Z_3^-, respectively, specified with respect to the *Pbam* basis. The one-dimensional nature of these representations implies an indispensable nonequivalence of the structures.

The relevant analysis indicates that, keeping the $PbZrO_3$ type of distortions as frozen modes, there are two ways that the same type of atomic displacement, doubling the *c* axis, can be incorporated into the structure. Difference between them is illustrated in Fig. 4, where the same displacive modes of Bi are incorporated into the tilted $PbZrO_3$ structure in two nonequivalent ways. In spite of the fact that both structures are characterized by the same space group and supercell, locally, they are essentially different and imply even different bond lengths and angles. The difference becomes clear if one compares the Bi displacements in the regions, marked with ellipses (Fig. 4), where octahedra are tilted in a similar way. As revealed by our DFT calculations, these structures are not degenerate in energy, in line with the symmetry arguments. The modification obtained from the starting coordinates of Ref. [3] with the origin choice at (1/2,3/2,0) and shown in Fig. 4 as "BFS2" (right panel) represents the ground state of BFS.

To compare the experimental [3] and calculated structures, we decomposed the distortions obtained in our calculation in terms of $Pm\bar{3}m$ cubic space group, by employing ISODISTORT software [21]. We present the results for the primary distortions obtained with the help of the GGA XC functional, which gives the best results in comparison with experiment [3], in Table II (see Tables 3S and 4S of the Supplemental Material [29] for the full mode's details) along with their experimental counterparts directly refined from the neutron diffraction data collected at $T = 1.5$ K (for details of this experiment see Ref. [3]).

All primary modes found experimentally appear in our calculations with the largest amplitudes and right signs, indicating a qualitatively good theoretical description. Note

TABLE II. Amplitudes of the primary modes for the experimental and calculated "BFS2" structures

Displacive mode	Experiment	GGA-frozen	GGA-rel
O(E_u) R_4^+	−2.853(15)	−2.636	−2.616
O(E_u)1 Σ_2	1.343(27)	1.009	1.038
O(E_u)2 Σ_2	−1.115(24)	−1.111	−1.112
Bi(T_{1u}) Σ_2	1.235(9)	1.193	1.282
O(E_u) S_4	−0.751(42)	−0.569	−0.571
O(E_u) T_4	−0.821(63)	−1.358	−1.374
Bi(T_{1u}) Λ_3	−0.683(23)	−0.734	−0.809

that the largest discrepancy is obtained for the T_4 oxygen mode which has the largest experimental uncertainty [3]. The largest distortion R_4^+ is antiphase octahedral tilting about the $[101]_p$ axis, and the rotation angle 14.09° found experimentally is very close to the value obtained by the structure relaxation, 13.06°. The calculated antiferroelectric displacement of Bi along this axis (Σ_2 mode) is also practically identical to the experimental value, 0.31 Å. The Λ_3 and T_4 modes describe antiferroelectric displacements of Bi along the b axis of the $Pnma$ space group ($[010]_p$ pseudocubic direction) and the "$++--$" octahedral tilting about the same axis, respectively. The corresponding experimentally determined distortions in the conventional units are 4.2° and 0.20 Å versus 6.8° and 0.21 Å of their theoretical counterparts. These modes are characteristic of the $\sqrt{2} \times 4 \times 2\sqrt{2}$ polymorphs. Apparently, a strong coupling between the Λ_3 and T_4 distortions is a specific property of Bi-based perovskites, which causes the stability of the $\sqrt{2} \times 4 \times 2\sqrt{2}$ $Pnma$ structure. This coupling is "predetermined" by the Σ_2 antiferroelectric mode through the trilinear free-energy invariant, $\zeta_1\zeta_2\zeta_3$, which couples the $\Sigma_2(\zeta_1)$, $\Lambda_3(\zeta_2)$, and $T_4(\zeta_3)$ order parameters.

Experimentally, it was found that the $Pnma$ structural modification competes with the two polar phases, $R3c$ and $Ima2$, in the BFS system [3]. A common feature of all these crystal structures is a combination of ferroelectric/antiferroelectric atomic displacements (vector distortions) with octahedral tilting (pseudovector distortions) about the same crystallographic directions. This structural feature points to the crucial role of the macroscopic strains since both types of distortion are coupled to the same strain components through the appropriate linear-quadratic invariants. For instance, in the $\sqrt{2} \times 4 \times 2\sqrt{2}$ $Pnma$ structure, the two macroscopic order parameters associated with $\Gamma_3^+(e_1)$ and $\Gamma_5^+(e_2)$ irreducible representations, which are $-e_{xx} - e_{zz} + 2e_{yy}$ (tetragonal compression/elongation along $[010]_p$) and e_{xz} (shear strain in the $(101)_p$ plane) symmetrized combinations of the macroscopic strains (see Tables 3S and 4S of the Supplemental Material [29]), respectively, are both coupled to the $R_4^+(\eta_1)$ and $\Sigma_2(\eta_2)$ order parameters as $e_i\eta_j^2$ $(i,j = 1,2)$. The same coupling scheme is applied to the octahedral tilting and polar displacements in the $Ima2$ polymorph [3].

In the polar rhombohedral modification $R3c$, the vector and pseudovector distortions are coupled to the $e_{xy} + e_{yz} + e_{xz}$ combination of the macroscopic strains. This means that external perturbations conjugated with the macroscopic strains (uniaxial pressure or misfit between substrate and sample film) are an extremely efficient way to control the phase stability in the BFS system. One additional parameter, the ratio between Fe and Sc, can also be tuned to bring the system to the verge of the phase balance where an enhanced functionality such as peizo-response and multiferroic properties are expected.

This work was partially supported by the Russian Foundation for Basic Research (Projects No. 12-08-00887_a, No. 14-02-90024 Bel_a, and No. 14-02-90438 Ucr_a), Ministry of education of Russian Federation (research project 2132, task No. 2014/174) and by the Belarus Republican Foundation for Basic Research (Project No. T14R-019). S.P. appreciates discussions with Laurent Bellaiche and acknowledges ONR Grants No. N00014-11-1-0384 and No. N00014-12-1-1034.

[1] D. A. Rusakov, A. M. Abakumov, K. Yamaura, A. A. Belik, G. Van Tendeloo, and E. Takayama-Muromachi, Chem. Mater. **23**, 285 (2011).

[2] A. A. Belik, A. M. Abakumov, A. A. Tsirlin, J. Hadermann, J. Kim, G. Van Tendeloo, and E. Takayama-Muromachi, Chem. Mater. **23**, 4505 (2011).

[3] D. D. Khalyavin, A. N. Salak, N. M. Olekhnovich, A. V. Pushkarev, Yu. V. Radyush, P. Manuel, I. P. Raevski, M. L. Zheludkevich, and M. G. S. Ferreira, Phys. Rev. B **89**, 174414 (2014)..

[4] S. Karimi, I. M. Reaney, I. Levin, and I. Sterianou, Appl. Phys. Lett. **94**, 112903 (2009).

[5] I. Levin, M. G. Tucker, H. Wu, V. Provenzano, C. L. Dennis, S. Karimi, T. Comyn, T. Stevenson, R. I. Smith, and I. M. Reaney, Chem. Mater. **23**, 2166 (2011).

[6] S. Trolier-McKinstry, M. D. Biegalski, J. L. Wang, A. A. Belik, E. Takayama-Muromachi, and I. J. Levin, Appl. Phys. **104**, 044102 (2008).

[7] C. J. Howard, R. L. Withers, K. S. Knight, and Z. Zhang, J. Phys.: Condens. Matter **20**, 135202 (2008).

[8] M. Yashima, S. Matsuyama, R. Sano, M. Itoh, K. Tsuda, and D. Fu, Chem. Mater. **23**, 1643 (2011).

[9] S. Prosandeev, D. Wang, W. Ren, J. Íñiguez, and L. Bellaiche, Adv. Funct. Mater. **23**, 234 (2013).

[10] Y. Yang, W. Ren, D. Wang, and L. Bellaiche, Phys. Rev. Lett. **109**, 267602 (2012).

[11] M. D. Peel, S. P. Thompson, A. Daoud-Aladine, S. E. Ashbrook, and P. Lightfoot, Inorg. Chem. **51**, 6876 (2012).

[12] R. Ranjan, D. Pandey, and N. P. Lalla, Phys. Rev. Lett. **84**, 3726 (2000).

[13] R. Garg, B. N. Rao, A. Senyshyn, and R. Ranjan, J. Appl. Phys. **114**, 234102 (2013).

[14] E. A. Eliseev, S. V. Kalinin, Y. Gu, M. D. Glinchuk, V. Khist, A. Borisevich, V. Gopalan, and L.-Q. Chen, and A. N. Morozovska, Phys. Rev. B **88**, 224105 (2013).

[15] A. Y. Borisevich, E. A. Eliseev, A. N. Morozovska, C.-J. Cheng, J.-Y. Lin, Y. H. Chu, D. Kan, I. Takeuchi, V. Nagarajan, and S. V. Kalinin, Nat. Commun. **3**, 775 (2012).

[16] M. Guennou, P. Bouvier, G. S. Chen, B. Dkhil, R. Haumont, G. Garbarino, and J. Kreisel, Phys. Rev. B **84**, 174107 (2011).

[17] M. Guennou, P. Bouvier, R. Haumont, G. Garbarino, and J. Kreisel, Phase Transitions **84**, 474 (2011).
[18] R. Haumont, P. Bouvier, A. Pashkin, K. Rabia, S. Frank, B. Dkhil, W. A. Crichton, C. A. Kuntscher, and J. Kreisel, Phys. Rev. B **79**, 184110 (2009).
[19] S. B. Emery, C.-J. Cheng, D. Kan, F. J. Rueckert, S. P. Alpay, V. Nagarajan, I. Takeuchi, and B. O. Wells, Appl. Phys. Lett. **97**, 152902 (2010).
[20] H. T. Stokes, D. M. Hatch, and B. J. Campbell, ISOTROPY software suite, http://iso.byu.edu
[21] B. J. Campbell, H. T. Stokes, D. E. Tanner, and D. M. Hatch, J. Appl. Crystallogr. **39**, 607 (2006).
[22] D. D. Khalyavin, A. N. Salak, N. P. Vyshatko, A. B. Lopes, N. M. Olekhnovich, A. V. Pushkarev, I. I. Maroz, Yu. V. Radyush, Chem. Mater. **18**, 5104 (2006).
[23] W. Kohn and L. J. Sham, Phys. Rev. **140**, A1133 (1965).
[24] V. I. Anisimov, F. Aryasetiawan, and A. I. Lichtenstein, J. Phys: Condens. Matter **9**, 767 (1997).
[25] G. Kresse and J. Furthmuller, Phys. Rev. B **54**, 11169 (1996); G. Kresse and D. Joubert, *ibid.* **59**, 1758 (1999).
[26] I. A. Kornev, S. Lisenkov, R. Haumont, B. Dkhil, and L. Bellaiche, Phys. Rev. Lett. **99**, 227602 (2007).
[27] J. P. Perdew, K. Burke, and M. Ernzerhof, Phys. Rev. Lett. **77**, 3865 (1996).
[28] I. P. Raevski, S. P. Kubrin, S. I. Raevskaya, D. A. Sarychev, S. A. Prosandeev, and M. A. Malitskaya, Phys. Rev. B **85**, 224412 (2012).
[29] See Supplemental Material at http://link.aps.org/supplemental/10.1103/PhysRevB.90.054110 for structural parameters and full mode decomposition details of BFS2 obtained by the structure relaxation.